

Supplementary Materials for
**Engineering of hybrid spheroids of mesenchymal stem cells and drug depots
for immunomodulating effect in islet xenotransplantation**

Tiep Tien Nguyen *et al.*

Corresponding author: Jee-Heon Jeong, jeeheon@skku.edu; Simmyung Yook, ysimmyung@kmu.ac.kr

Sci. Adv. **8**, eabn8614 (2022)
DOI: 10.1126/sciadv.abn8614

The PDF file includes:

Figs. S1 to S19
Tables S1 and S2
Captions for Source Data File

Other Supplementary Material for this manuscript includes the following:

Source data file S1

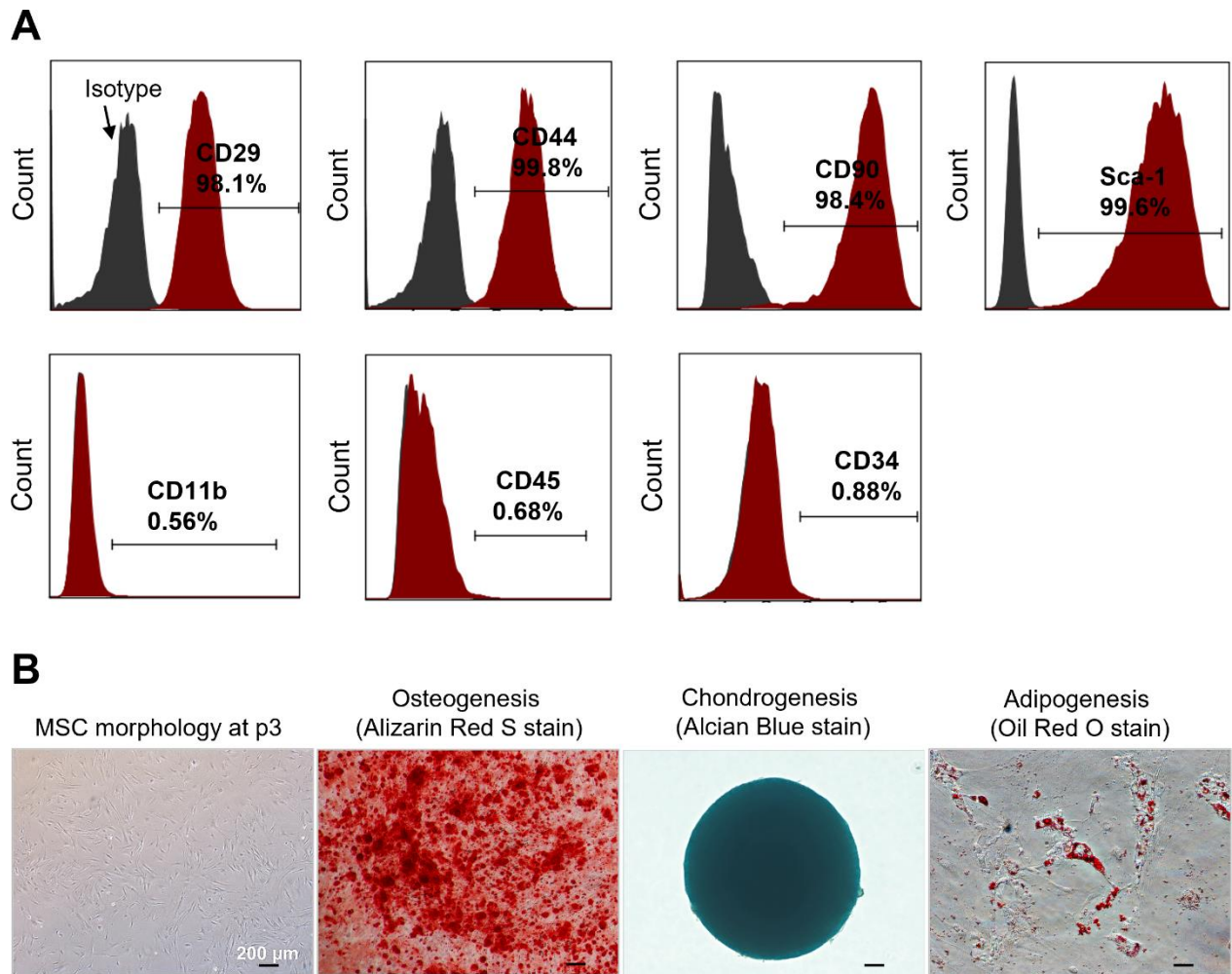


Fig. S1. Characterization of MSCs isolated from subcutaneous adipose tissues of C57BL/6 mice. (A) Evaluation of surface markers by flow cytometry. The MSC phenotype is positive (>95%) for CD29, CD44, CD90, and Sca-1 but negative (<2%) for CD11b, CD34, and CD45. Samples stained with respective isotype control antibodies served as controls. (B) Differentiation of MSCs into three lineages (osteogenic cells, chondrogenic cells, and adipogenic cells). The first image on the left shows the morphology of MSCs cultured to passage 3.

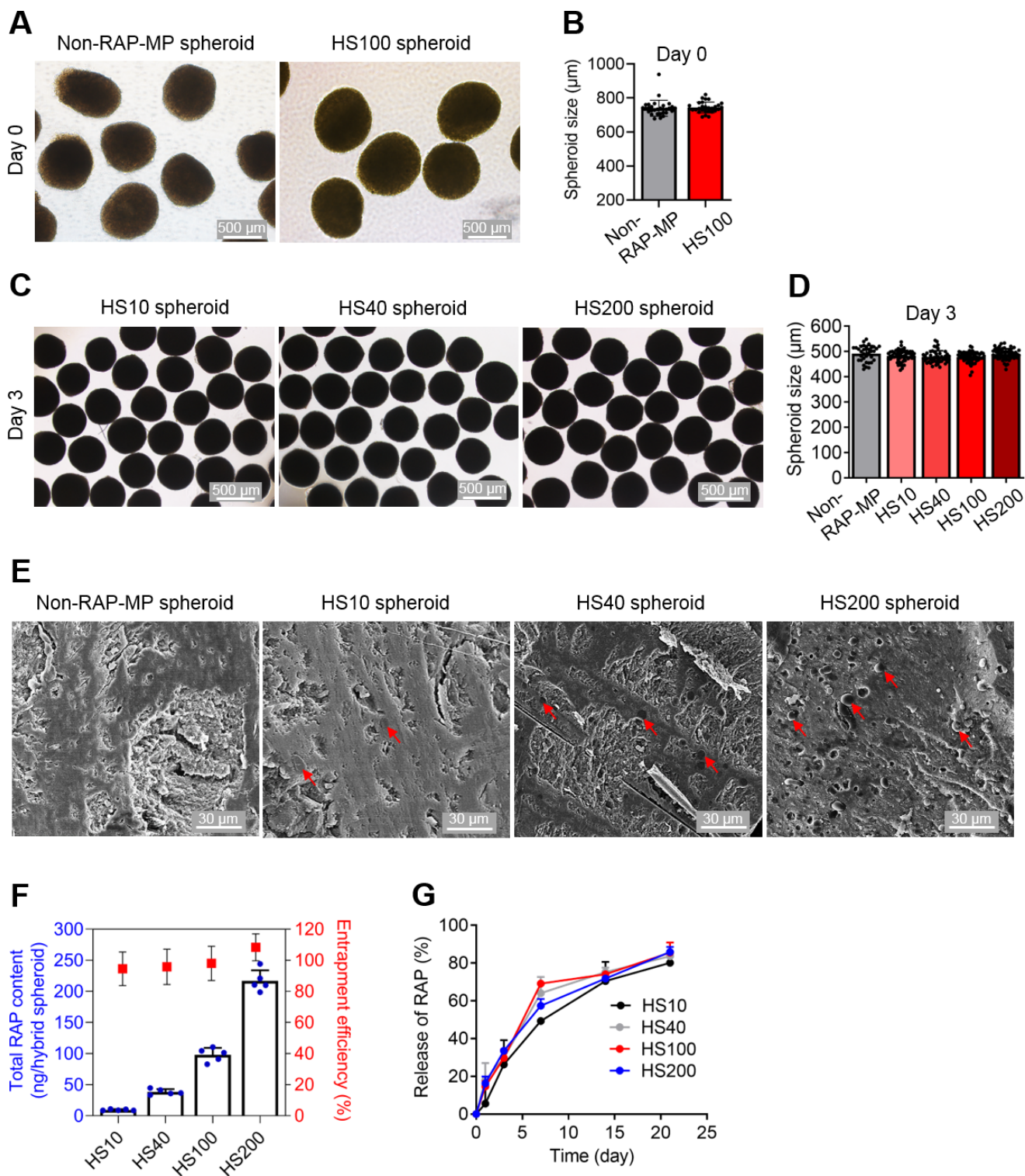


Fig. S2. Methylcellulose-based fabrication of MSC spheroids. (A, B) Images and sizes of non-RAP-MP and HS100 spheroids at day 0. Scale bar: 500 μm. (C, D) The images and sizes HS10, HS40, HS200 spheroids after 3 days of culture. Scale bar: 500 μm. (E) SEM images of non-RAP-MP and hybrid

spheroids. The red arrows indicate RAP-MPs. Scale bar: 30 μm . **(F)** Total RAP contents (ng) and entrapment efficiencies (%) in hybrid spheroids. **(G)** Release kinetics of RAP from hybrid spheroids. Data shown in **(F)** and **(G)** are means \pm SDs of 2-5 samples.

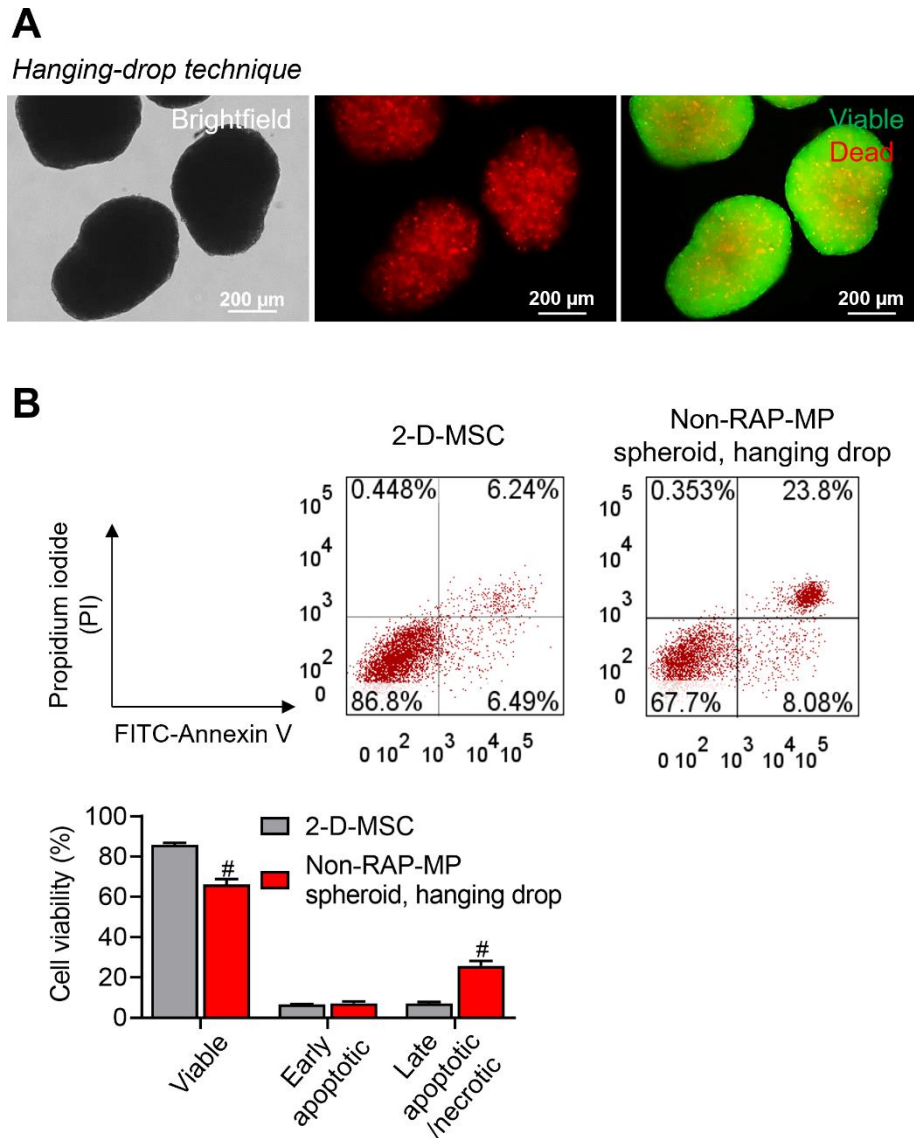


Fig. S3. Viability of MSCs in spheroids after culture for 3 days. (A) Live/dead staining assay. Viable and dead cells were shown by green (acridine orange) and red (propidium iodide), respectively. Scale bar: 200 μ m. (B) Flow cytometry-based quantitative assay (n=3 independent experiments). Data are expressed as means \pm SDs and were analyzed using the unpaired two-tailed t-test. [#]p < 0.001 vs 2-D-MSC group.

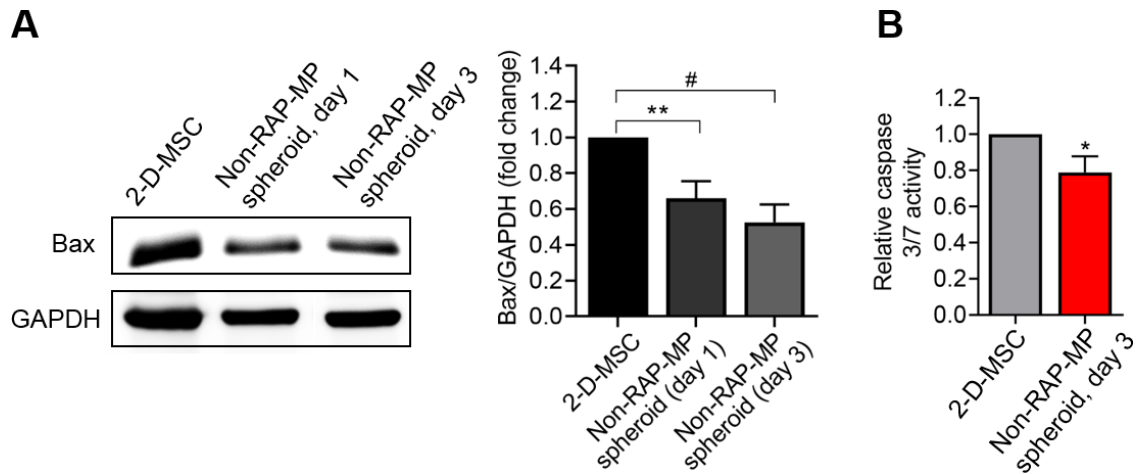


Fig. S4. Assessment of apoptotic events in MSCs cultured as monolayers (2-D) or spheroids fabricated in methylcellulose medium. (A, B) Determination of Bax level by western blot and determination of Caspase 3/7 activity, respectively. Data are expressed as means \pm SDs of 3 independent assays and were analyzed using (A) one-way ANOVA and (B) unpaired two-tailed t-test. * $p < 0.05$, ** $p < 0.01$, # $p < 0.001$ vs 2-D-MSC group.

and flow cytometry-based quantitative assay (n=3 independent assays), respectively. Scale bar: 200 μ m. (C) Determination of Bax level by western blot; n=6 independent assays for non-RAP-MP spheroid and HS100 spheroid groups, n=3 independent assays for HS10, HS40 and HS200 spheroid groups. (D) Determination of Caspase 3/7 activity; n=3 independent assays. Data in (B, C, D) are expressed as means \pm SDs and were analyzed using one-way ANOVA; * p < 0.05, ** p < 0.01, #p < 0.001, \$p < 0.0001 vs non-RAP-MP spheroid group.

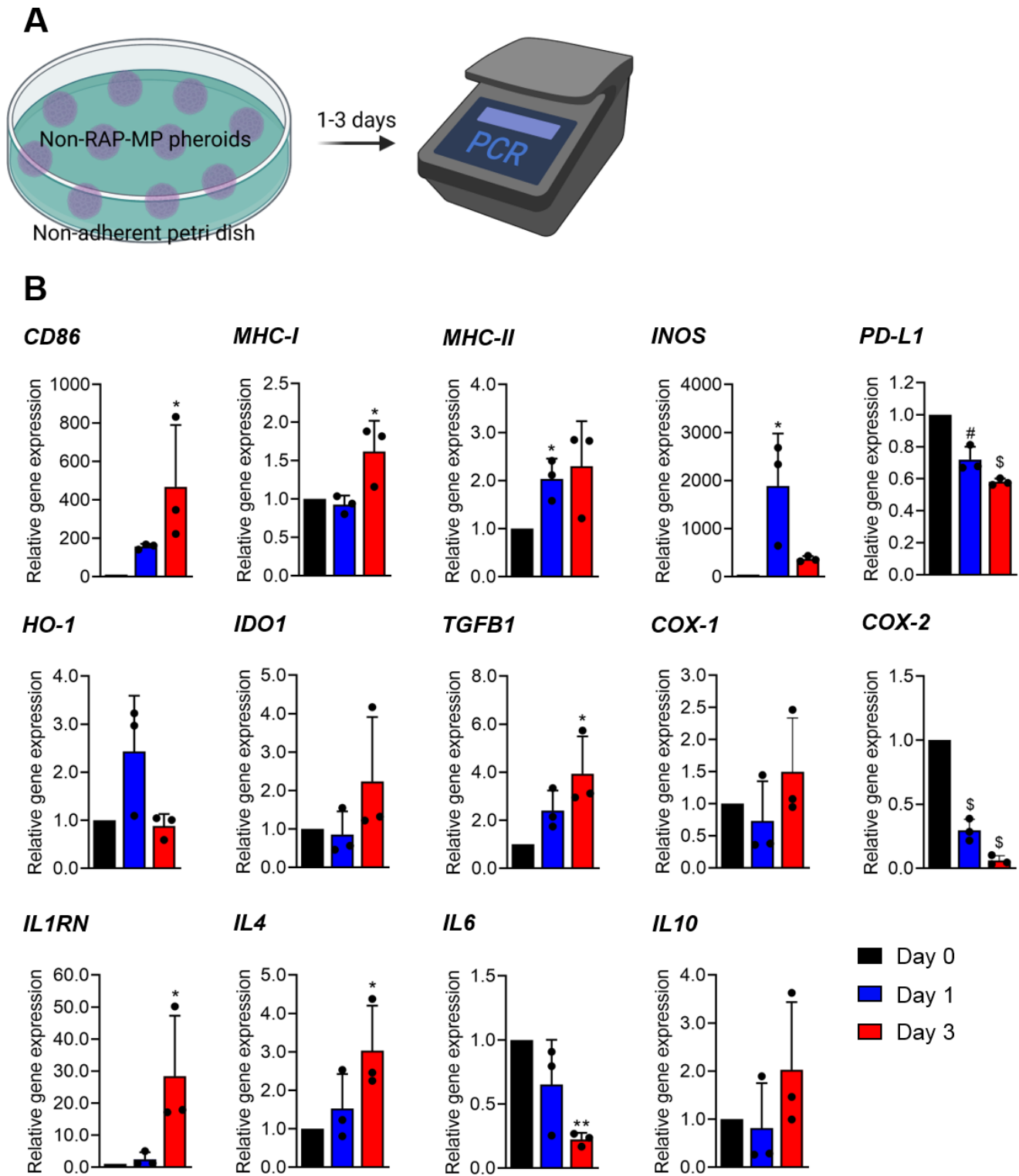


Fig. S6. Assessment of dynamic changes in immune-related gene expressions of non-RAP-MP spheroids cultured under a non-stimulating condition (no cytokine cocktail treatment). (A) Graphical illustration of spheroid culture and analysis. **(B)** Gene expression levels as determined by qRT-

PCR. Data are expressed as the means \pm SDs of 3 independent experiments and were analyzed using one-way ANOVA. * $p < 0.05$, ** $p < 0.01$, # $p < 0.001$, \$ $p < 0.0001$ vs day 0 (2-D-MSCs).

The data are expressed as the means \pm SDs of 3 independent experiments and were analyzed using the unpaired two-tailed t-test. *p < 0.05, **p < 0.01 vs non-stimulated cells.

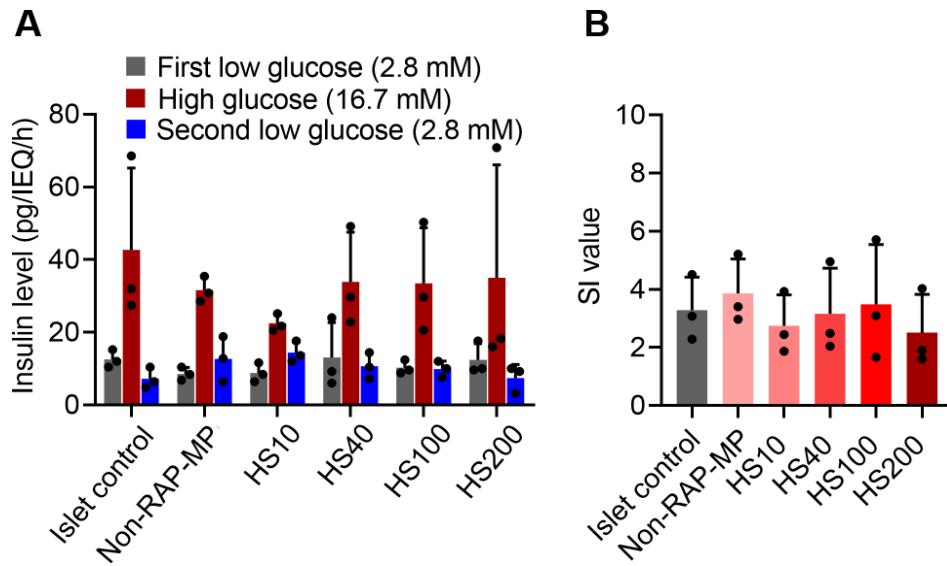


Fig. S8. Assessment of functionality of islets after co-culture with spheroids, using glucose-stimulated insulin secretion (GSIS) assay. (A) Absolute levels of insulin released by islets after three cycles (low-high-low) of glucose exposure (n=3). (B) Stimulation index (SI) values of control and different spheroid-treated groups. The SI values were calculated by dividing insulin level in high-glucose treatment to that in low-glucose treatment. The data were analyzed using one-way ANOVA.

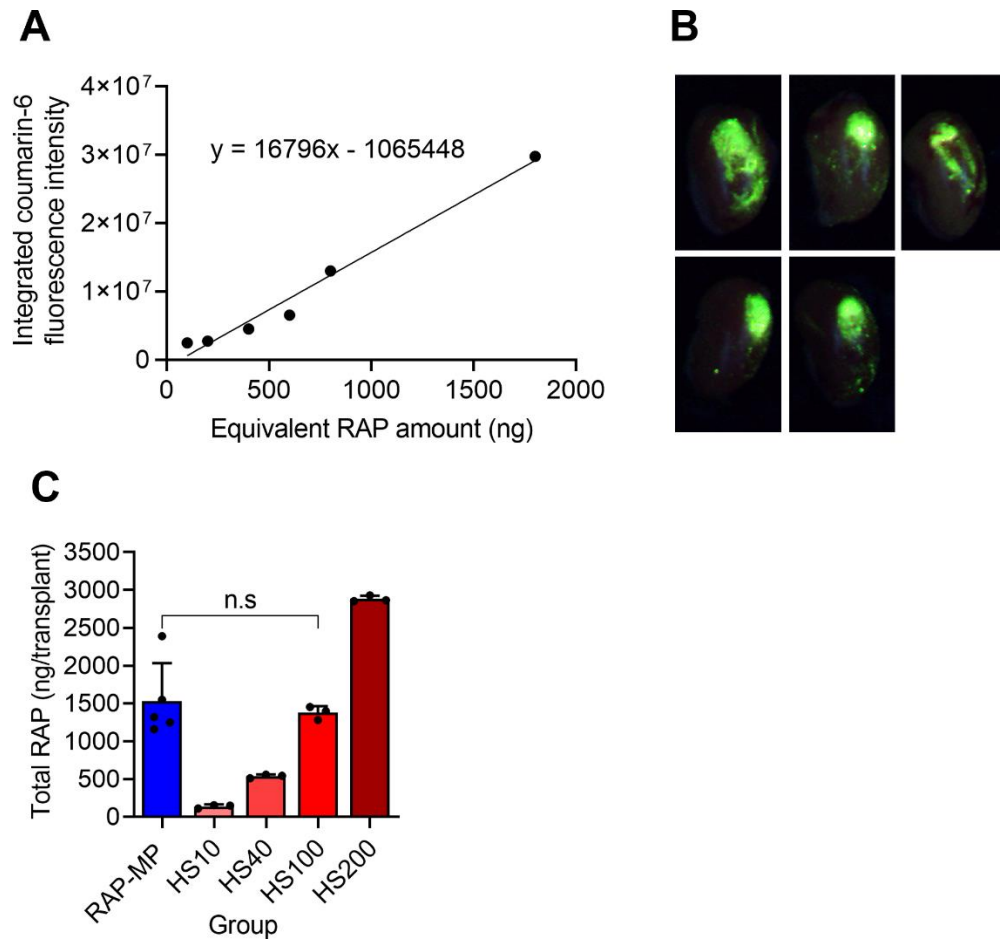


Fig. S9. Localization efficiency of RAP-MPs in islet grafts. Coumarin-6 was used to label RAP-MPs. (A) Calibration curve showing the relationship between fluorescence intensities and amounts of RAP-MPs, which were equivalent to 100-1800 ng RAP. (B) Fluorescence images of kidneys bearing islet grafts, and theoretically, 50 μ g of RAP-MPs (equivalent to 2000 ng of RAP, given a RAP loading capacity of RAP-MPs of ~4%; n=5 mice). Signals were detected in the GFP channel of a Fluorescence In Vivo Imaging (FOBI) system. (C) Calculation of total RAP doses per recipient of islets plus RAP-MPs or islets plus hybrid spheroids with different RAP loadings. The localization efficiency of RAP-MPs into islet grafts was calculated ~75%. The actual doses of RAP in the RAP-MP and HS100 spheroid groups were non-significantly different (n.s) as determined by the unpaired two-tailed t-test.

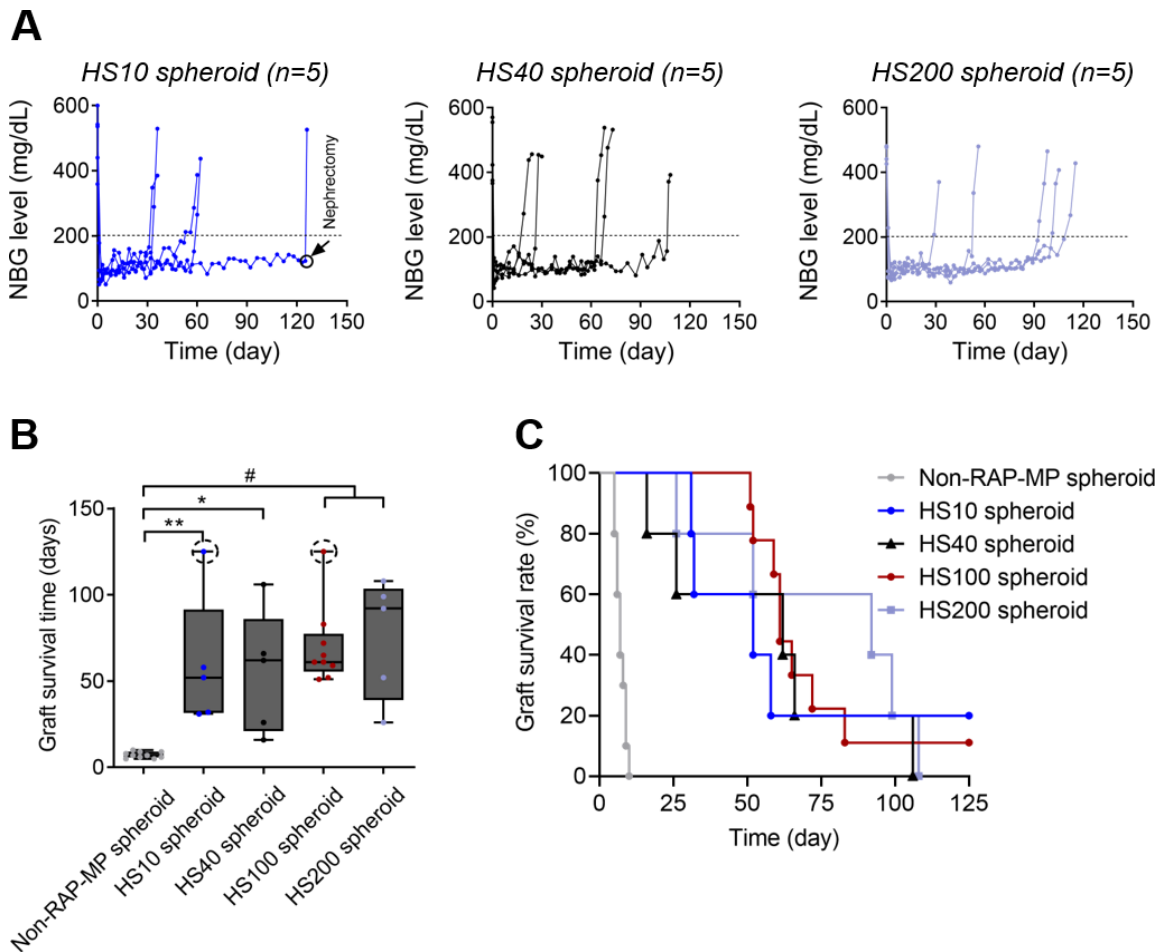


Fig. S10. Locoregional delivery of hybrid spheroids promotes islet xenograft survival in the diabetic C57BL/6 mouse model. Mice received a transplantation of islets with HS10, HS40, or HS200 spheroids. **(A)** NBG observation test. The circle and the arrow indicate the time of functional islet retrieval (day 125). **(B, C)** Islet xenograft survival times (day) and survival rates (%) as demonstrated by floating bars and Kaplan-Meier curves, respectively. The data in **(B)** were analyzed using one-way ANOVA; * $p < 0.05$, ** $p < 0.01$, # $p < 0.001$ vs non-RAP-MP spheroid group. The dashed circles indicate mice with functional islet grafts at day 125 after transplantation.

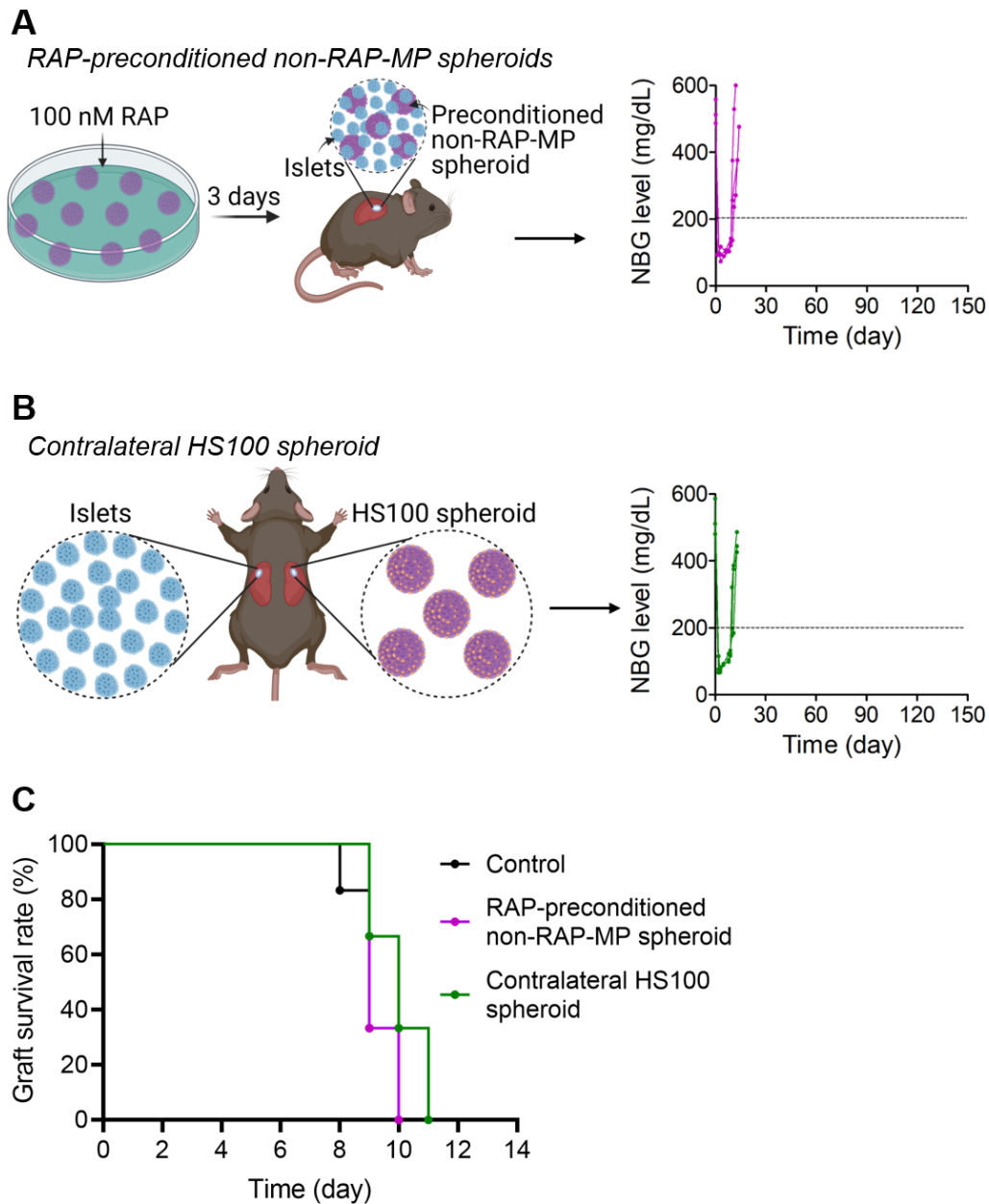


Fig. S11. Requirement of locoregionally delivered hybrid spheroids to enhance islet xenograft survival time. (A) NBG testing in mice that received the transplantation of islets and non-RAP-MP spheroids that had been preconditioned with 100 nM RAP solution for 3 days (n=3). (B) NBG testing in mice that received separate transplantation of islets and HS100 spheroids under capsules of contralateral kidneys (n=3). (C) Kaplan-Meier curves of islet xenograft survival rate (%).

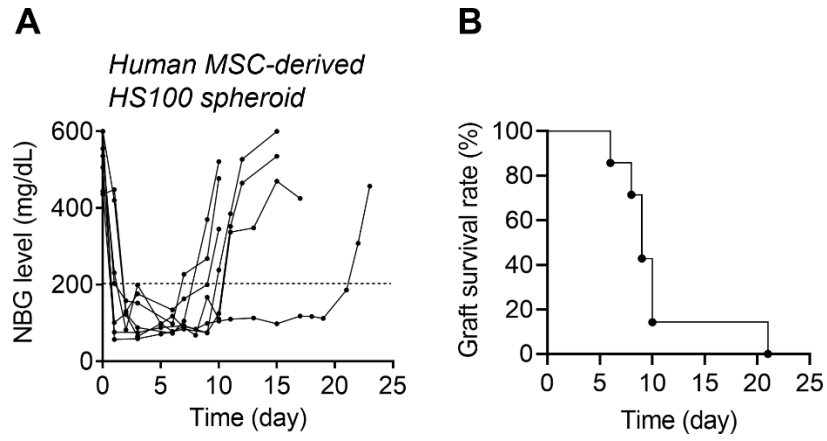


Fig. S12. Locoregional delivery of hybrid spheroids derived from human MSCs fails to prevent the early rejection of islet xenografts. (A) NBG test results (n=7). (B) Kaplan-Meier curve of islet xenograft survival rate (%).

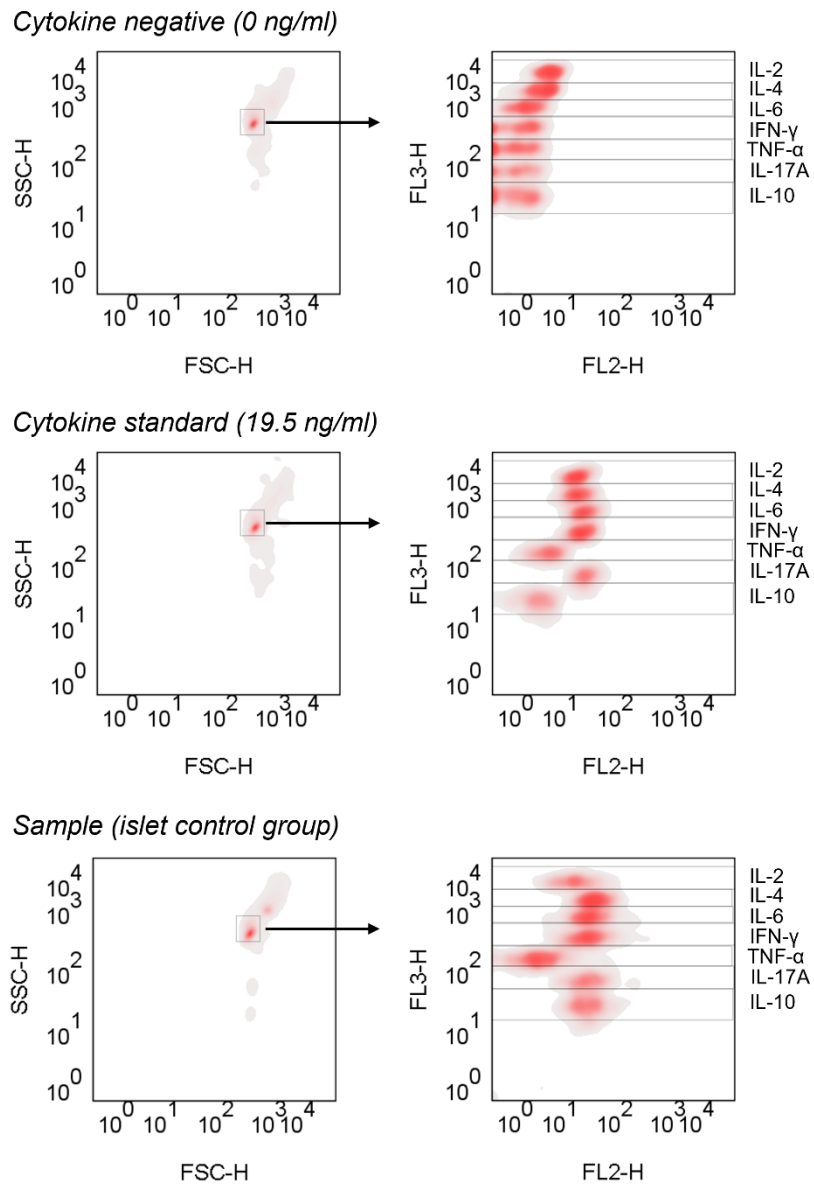


Fig. S13. Flow cytometry gating strategy for the assessment of cytokine levels in mouse serum samples. Flow cytometric conditions were optimized according to the manufacturer's instructions (Thermo Fisher Scientific, Waltham, MA, USA).

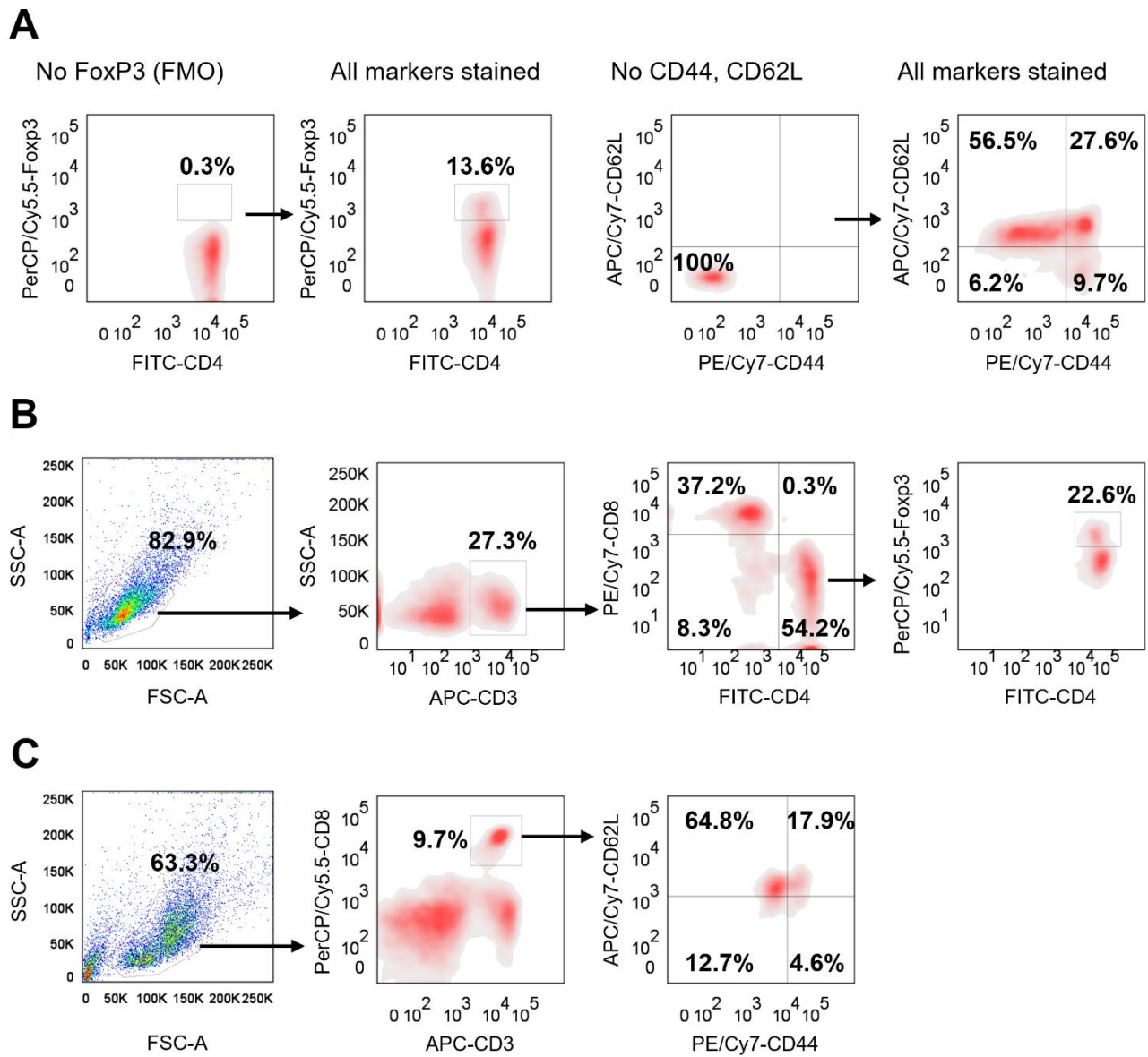


Fig. S14. Flow cytometry gating strategy for the assessment of T-cell populations in mouse lymphoid organs. (A) Optimization of flow cytometric conditions using fluorescence minus one (FMO) and isotype control samples. (B, C) CD3⁺ T cells were gated from total cells. CD4⁺ and CD8⁺ T cells were gated from the CD3⁺ T cell population, and then, CD4⁺ FoxP3⁺ T cells, effector memory CD8⁺ T cells (T_{EM}; CD8⁺CD44^{high}CD62L^{low}), and central memory CD8⁺ T cells (T_{CM}; CD8⁺CD44^{high}CD62L^{high}) were gated.

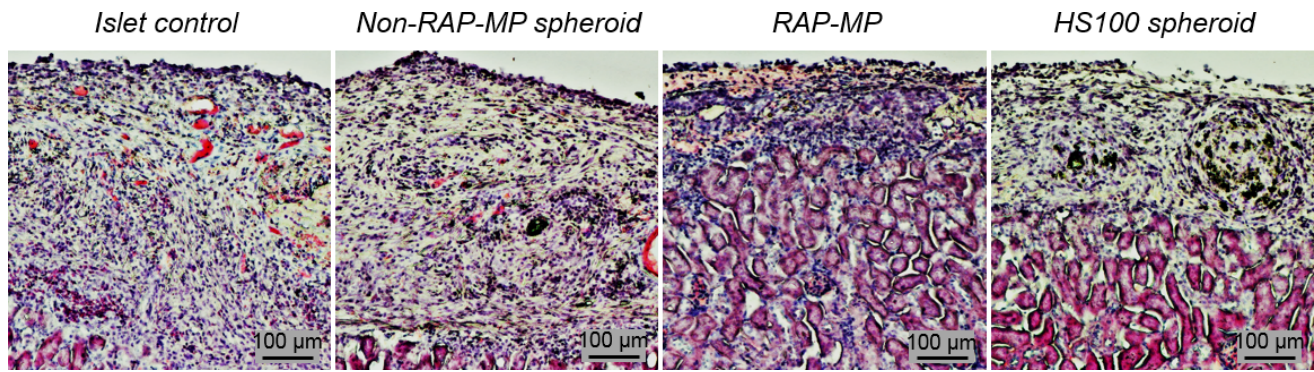


Fig. S15. Hematoxylin & eosin (H&E) staining of islet xenografts at 12 days post-transplantation.

Scale bar: 100 μm.

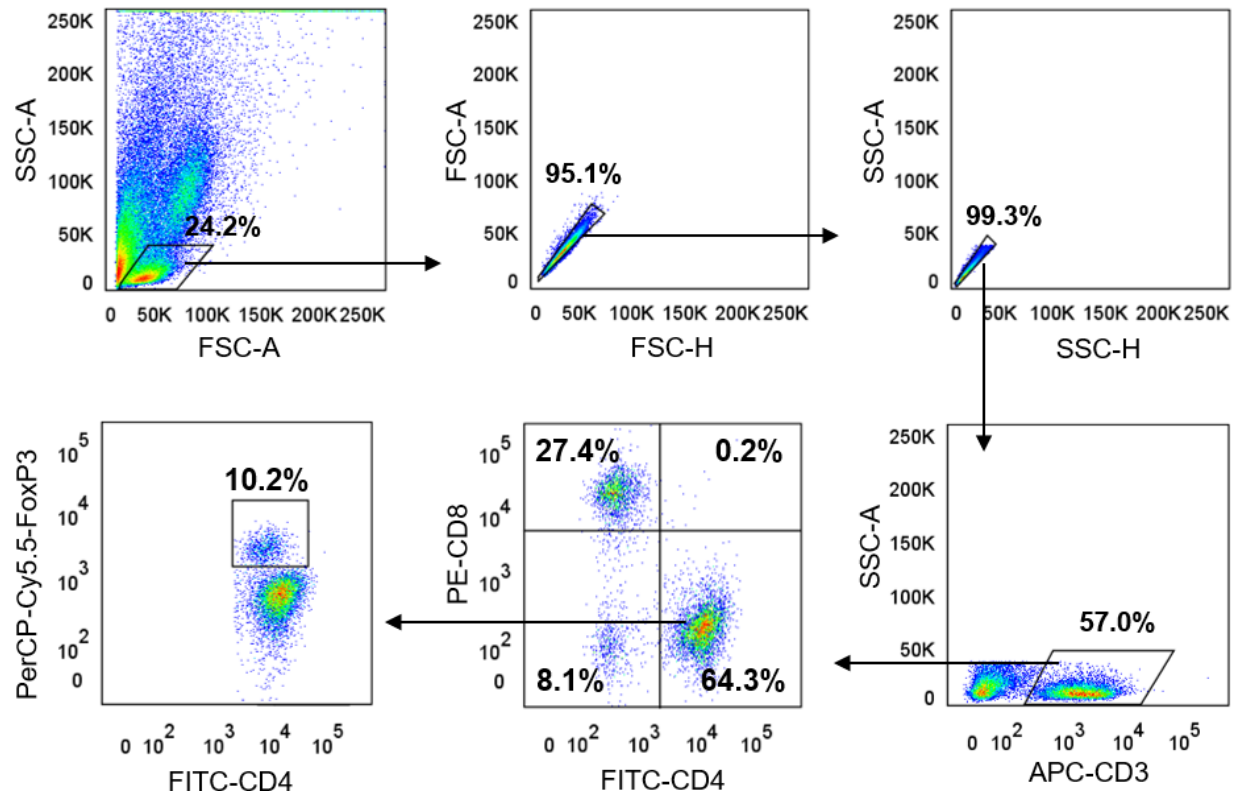


Fig. S16. Flow cytometry gating strategy for the assessment of T-cell populations in islet xenografts.

Doublet exclusion was performed on total gated cells. CD3⁺ T cells were gated from singlet signals, and CD4⁺ and CD8⁺ T cells were gated from the CD3⁺ T cell population. CD4⁺ FoxP3⁺ T cells were then gated.

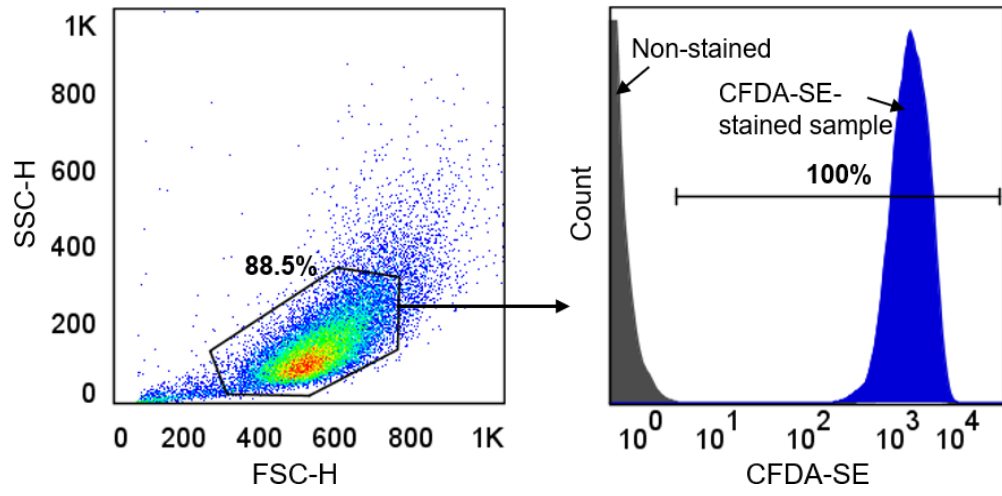


Fig. S17. Labeling of MSCs with CFDA-SE for *in vivo* tracking. The labeling efficiency of MSCs was 100%.

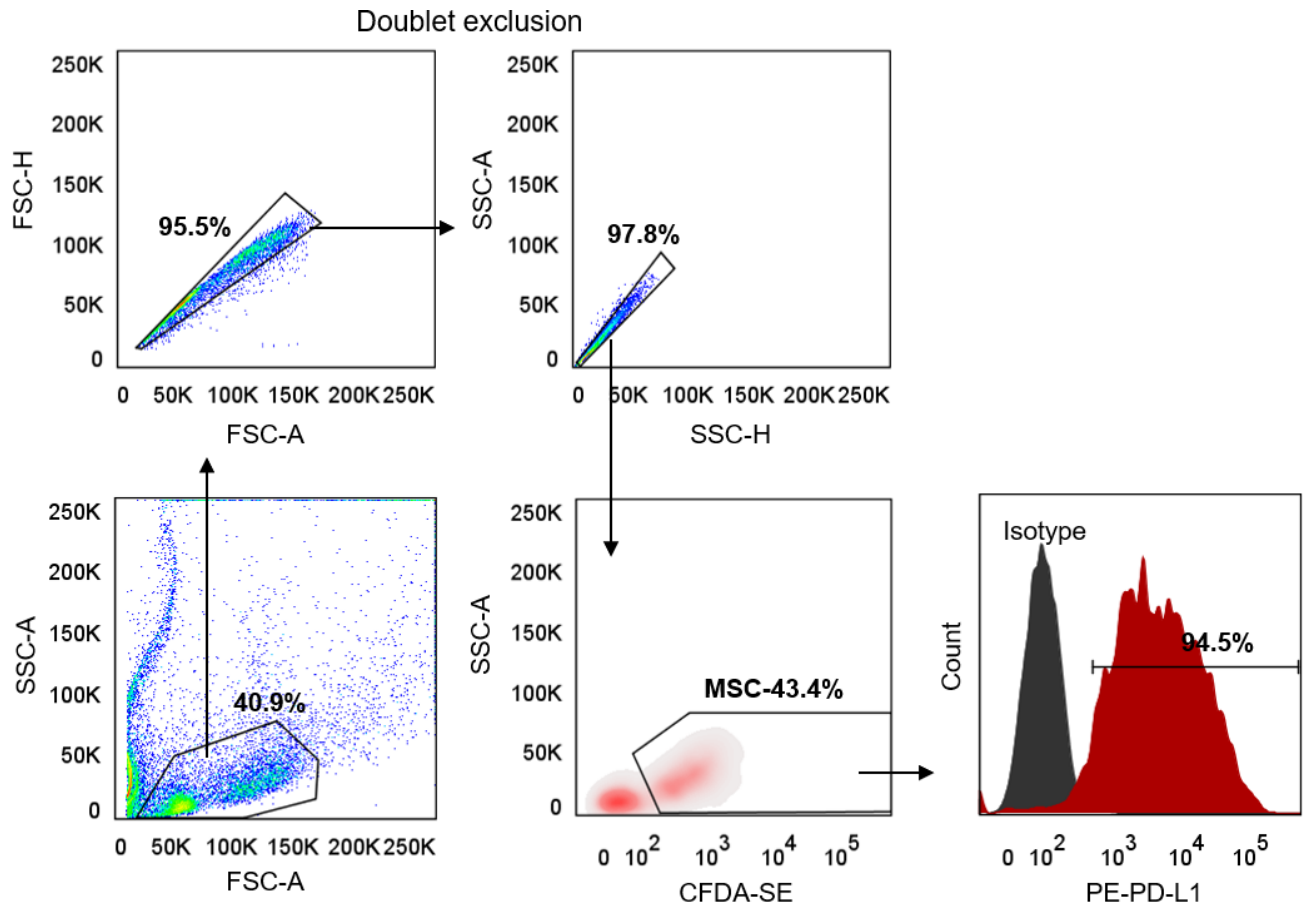


Fig. S18. Flow cytometry gating strategy for the assessment of MSC populations in islet xenografts.

Doublet exclusion was performed on total gated cells. The CFDA-SE⁺ MSC population was gated from singlet signals. CFDA-SE⁺ PD-L1⁺ MSCs were gated to assess the expression of PD-L1 by transplanted MSCs. PD-L1⁻ and PD-L1⁺ regions were differentiated using respective isotype control sample.

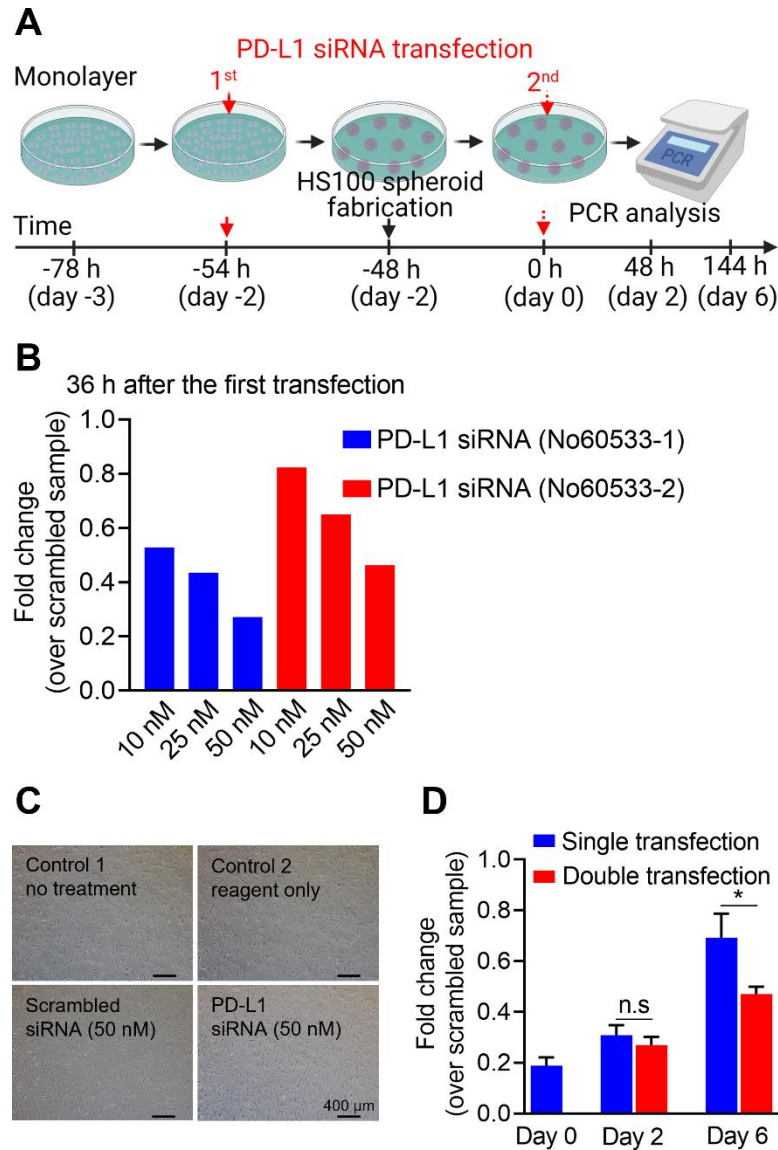


Fig. S19. Inhibition of PD-L1 expression in MSCs by PD-L1 siRNA. (A) Schematic of the transfection and assessment procedure. (B) Selection of a PD-L1 siRNA sequence for transfection. The PD-L1 siRNA sequence (code No. 60533-1) was selected from two sequences provided by Bioneer (Daejeon, Republic of Korea) based on its higher transfection efficiency. (C) Brightfield images of MSCs at 48 h after first transfection. Control cells were untreated (control 1) or treated with Lipofectamine RNAiMAX transfection reagent only (control 2). For the experiment, cells were transfected with scrambled siRNA (50 nM) or PD-L1 siRNA (50 nM). All treated cells had

a normal morphology and attachment properties similar with control 1 group, indicating no transfection-associated toxicity. Scale bar: 400 μm . **(D)** Transfection efficiencies and durations. Samples were transfected once or twice. PD-L1 expressions are shown as fold changes versus scrambled samples. Data are the means \pm SDs of 2 to 3 independent experiments and were analyzed using the unpaired two-tailed t-test; n.s non-significance, * $p < 0.05$.

Table S1. Primers used for qRT-PCR

Gene	Forward primer sequence	Reverse primer sequence
<i>COX-1</i>	TCGGAGCCCCAGATATAGCA	TTTCCGGCTAGAGGTGGGTA
<i>COX-2</i>	GGGCTCAGCCAGGCAGCAAAT	GCACTGTGTTTGGGGTGGGCT
<i>IL1RN</i>	TAGCAAATGAGCCACAGACG	ACATGGCAAACAACACAGGA
<i>IL4</i>	TCAACCCCCAGCTAGTTGTC	TGTTCTTCGTTGCTGTGAGG
<i>IL6</i>	ACAACCACGGCCTTCCCTACTT	CACGATTTCCCAGAGAACATGTG
<i>IL10</i>	CCAGGGAGATCCTTTGATGA	CATTCCCAGAGGAATTGCAT
<i>TGFB1</i>	TTGCTTCAGCTCCACAGAGA	TGGTTGTAGAGGGCAAGGAC
<i>IDO1</i>	GCTTTGCTCTACCACATCCAC	CAGGCGCTGTAACCTGTGT
<i>INOS</i>	GCTCGCTTTGCCACGGACGA	AAGGCAGCGGGCACATGCAA
<i>HO-1</i>	GGTGATGGCTTCCTTGTACC	AGTGAGGCCCATACCAGAAG
<i>MHC-I</i>	GGCAATGAGCAGAGTTTCCGAG	CCACTTCACAGCCAGAGATCAC
<i>MHC-II</i>	GTGTGCAGACACAACACTACGAGG	CTGTCACTGAGCAGACCAGAGT
<i>CD86</i>	GATTATCGGAGCGCCTTTCT	CCACACTGACTCTTCCATTCTT
<i>PD-L1</i>	TGCGGACTACAAGCGAATCACG	CTCAGCTTCTGGATAACCCTCG
<i>PRF1</i>	TCATCATCCCAGCCGTAGT	ATTCATGCCAGTGTGAGTGC
<i>GRMB</i>	ACTCTTGACGCTGGGACCTA	AGTGGGGCTTGACTTCATGT
<i>IFNG</i>	TTCTTCAGCAACAGCAAGGC	TCAGCAGCGACTCCTTTTCC
<i>TNF</i>	TAGCCAGGAGGAGAACAGAAAC	CCAGTGAGTGAAAGGGACAGAAC
<i>FOXP3</i>	CCTGGTTGTGAGAAGGTCTTCG	TGCTCCAGAGACTGCACCACTT
<i>GAPDH</i>	ACCACAGTCCATGCCATCAC	TCCACCACCCTGTTGCTGTA
<i>18S RNA</i>	TCAACACAGGGATCGGACAACACA	GCCTTGGATCAAGTTCACAGGCAA

Table S2. Antibody sources used in the study

Antibodies	Source	Catalogue	RRID
Rabbit anti-FoxP3	Cell Signaling	Cat# 12653S	AB_2797979
Rabbit anti-CD3	Novus Biologicals	Cat# NB600-1441	AB_789102
Rabbit anti-insulin H-86	Santa Cruz	Cat# sc-9168	AB_2126540
Mouse anti-insulin	ProteinTech	Cat# 66198-I-Ig	
Rabbit anti-BAX	Cell Signaling	Cat# 5023S	AB_10557411
Rabbit anti-GAPDH	Cell Signaling	Cat# 2118S	AB_561053
Anti-PD-L1 PE	BioLegend	Cat# 155404	AB_2728223
Anti-CD3 APC	BioLegend	Cat# 100236	AB_2561456
Anti-CD4 FITC	BioLegend	Cat# 100510	AB_312713
Anti-CD8a PE/Cy7	BioLegend	Cat# 100722	AB_312761
Anti-CD8a PE	BioLegend	Cat# 100707	AB_312746
Anti-CD44 PE/Cy7	BioLegend	Cat# 103029	AB_830786
Anti-CD90.2 FITC	BioLegend	Cat# 140303	AB_10642686
Anti-CD62L APC/Cy7	BioLegend	Cat# 104427	AB_830798
Anti-Sca-1 APC/Cy7	BioLegend	Cat# 108125	AB_10639725
Anti-CD34 APC	BioLegend	Cat# 119309	AB_1236482
Anti-FoxP3 PerCP-Cy5.5	BD Biosciences	Cat# 563902	AB_2630318
Anti-CD29 FITC	BioLegend	Cat# 102205	AB_312882
Anti-CD11b APC	BioLegend	Cat# 101212	AB_312795
Anti-CD45 PE	BioLegend	Cat# 103105	AB_312970
TrueStain anti-CD16/32	BioLegend	Cat# 101320	AB_1574975

Caption for Source data file

Figure 1.

(B) Size distribution of RAP-MPs. More than 200 particles were measured.

(D) *In vitro* release profile of RAP from RAP-MPs incubated in phosphate-buffered saline (PBS; pH 7.4, plus 1% Tween-20) at 37°C and 150 rpm.

Figure 2.

(C) Sizes of non-RAP-MP and HS100 spheroids.

(F) Actual contents of RAP in HS100 spheroids with respect to culture time, and cumulative RAP release percentages.

(H) Assessment of MSC viability in spheroids as determined by flow cytometry.

(I) Assessment of apoptotic events in spheroids based on western blot determination of Bax level.

(J) Assessment of apoptotic events in spheroids based on determination of Caspase 3/7 activity.

Figure 3.

(B) Gene expression levels in non-RAP-MP and HS100 spheroids with and without cytokine cocktail (interferon gamma-IFN- γ and tumor necrosis factor alpha-TNF- α) treatment.

Figure 4.

(B) Non-fasting blood glucose (NBG) levels of recipient mice.

(C) Islet xenograft survival times. "0" indicates mice with functional islet graft, whereas "1" indicates mice with rejected graft.

(D) Intraperitoneal glucose tolerance test (IPGTT) results at 12 days post-transplantation.

(E) Area under the curve of IPGTT results.

Figure 5.

(A) Serum levels of cytokines, determined using cytometric bead array (CBA) mouse Th1/Th2/Th17 cytokine kit.

(B) Serum IFN- γ /IL-10 ratios.

(C) Percentages of T cell populations on total gated cells in draining lymph nodes (DLNs) and spleen (SPLs), determined by flow cytometry.

Figure 6.

(B) Relative expressions of genes encoding for perforin (*PRF1*), granzyme B (*GRMB*), IFN- γ (*IFNG*), TNF- α (*TNF*), IL-10 (*IL10*), TGF- β 1 (*TGFB1*), and FoxP3 (*FOXP3*) in islet grafts.

(D) Flow cytometry of T cell populations in the RAP-MP and HS100 spheroid groups in islet grafts.

Figure 7.

(B) Retention of green fluorescence protein (GFP)-expressing MSCs in islet xenografts over time (values are residual GFP intensities).

(C) Relative gene expression of *PD-L1* in whole grafts containing islets and non-RAP-MP or HS100 spheroids at 12 days post-transplantation.

The effect of anti-PD-L1 antibody treatment on mice co-transplanted with islets and HS100 spheroids: (E) NBG test results, and (F) Islet xenograft survival times; "0" indicates mice with functional islet graft, whereas "1" indicates mice with rejected graft.

(G) *In vitro* PD-L1 protein expressions on MSCs in non-RAP-MP and HS100 spheroids with and without a cytokine cocktail treatment for 3 days, determined by flow cytometry.

(H) *In vivo* PD-L1 protein expressions on MSCs in non-RAP-MP and HS100 spheroids at 7 days post-transplantation, determined by flow cytometry.

Effect of MSC-mediated PD-L1 on islet xenograft survival: **(J)** NBG test results, and **(K)** Islet xenograft survival times; "0" indicates mice with functional islet graft, whereas "1" indicates mice with rejected graft.

Figure S2.

(B) Sizes of non-RAP-MP and HS100 spheroids at day 0.

(D) Sizes HS10, HS40, HS200 spheroids after 3 days of culture.

(F) Total RAP contents (ng) and entrapment efficiencies (%) in hybrid spheroids.

(G) Release kinetics of RAP from hybrid spheroids.

Figure S3.

(B) Viability of MSCs in spheroids after culture for 3 days, assessed by flow cytometry.

Figure S4.

(A) Assessment of apoptotic events in MSCs cultured as monolayers (2-D) or spheroids fabricated in methylcellulose medium, via determination of Bax level by western blot.

(B) Assessment of apoptotic events in MSCs cultured as 2-D or spheroids fabricated in methylcellulose medium, via determination of Caspase 3/7 activity.

Figure S5.

(B) Assessment of MSC viability in spheroids, determined by flow cytometry.

(C) Assessment of MSC apoptosis in spheroids, via determination of Bax level by western blot.

(D) Assessment of MSC apoptosis in spheroids, via determination of Caspase 3/7 activity.

Figure S6.

(B) Assessment of dynamic changes in immune-related gene expressions of non-RAP-MP spheroids cultured under a non-stimulating condition (no cytokine cocktail treatment).

Figure S7.

(B) Assessment of dynamic changes in immune-related gene expressions in non-RAP-MP spheroids cultured under a stimulating condition (with a cytokine cocktail).

Figure S8.

(A) Absolute levels of insulin released by islets after three cycles (low-high-low) of glucose exposure.

(B) Stimulation index values of control and different spheroid-treated groups.

Figure S9.

(A) Amounts and respective fluorescence intensities of RAP-MPs in islet grafts, used for developing a calibration curve.

(C) Calculation of total RAP doses per recipient of islets plus RAP-MPs or islets plus hybrid spheroids with different RAP loadings.

Figure S10.

Locoregional delivery of different hybrid spheroids to islet grafts.

(A) NBG test results.

(B, C) Islet xenograft survival times; "0" indicates mice with functional islet graft, whereas "1" indicates mice with rejected graft.

Figure S11.

(A) NBG testing in mice that received the transplantation of islets and non-RAP-MP spheroids that had been preconditioned with 100 nM RAP solution for 3 days.

(B) NBG testing in mice that received separate transplantation of islets and HS100 spheroids under capsules of contralateral kidneys.

(C) Islet xenograft survival times; "0" indicates mice with functional islet graft, whereas "1" indicates mice with rejected graft.

Figure S12.

Locoregional delivery of hybrid spheroids derived from human MSCs to islet graft.

(A) NBG test results.

(B) Islet xenograft survival times; "0" indicates mice with functional islet graft, whereas "1" indicates mice with rejected graft.

Figure S19.

Inhibition of PD-L1 expression in MSCs by PD-L1 siRNA.

(B) Transfection efficiencies of different PD-L1 siRNA sequences at different concentrations.

(D) Transfection efficiencies with respect to culture time of single and double transfection approaches.